Evaluation of DEM size and grid spacing for fluvial patch-scale roughness parameterisation

Jane Groom, Stéphane Bertin, Heide Friedrich

Evaluation of DEM size and grid spacing for fluvial patch-scale roughness parameterisation.

Jane Groom (jgro800@aucklanduni.ac.nz),

Stephane Bertin (s.bertin@ymail.com) and

Heide Friedrich (h.friedrich@auckland.ac.nz)

Department of Civil and Environmental Engineering, University of Auckland, Auckland, New Zealand.

Highlights

- Facilitates the improvement of understanding the analysis of topographic data
- A single roughness parameter is inadequate for describing patch-scale roughness
- A DEM size exceeding 16 x D_{50A} is appropriate to characterise grain-roughness
- Grid spacing should reflect the scale of research
- This analysis can be used on a variety of applications using topographic data

Abstract

Surface roughness is a term used in fluvial research without an unanimousdefinition, and clarification of the term and improved parameterisation is needed in future research. Improvements to the collection of topographic data, using photogrammetry, have provided accurate digital elevation models (DEMs) of field and laboratory gravel-bed patches. In this study, we use a moving-window process for analysing spatial variability within DEMs. Using this information, and in unison, we consider the effect of DEM size and grid spacing on an extensive range of roughness parameters, in order to provide insights for obtaining grain-

roughness statistics. We show that DEM size influences the calculated roughness statistics, and the observation of plateaus in statistics for DEM window sizes above 16 × D_{50A} in both directions (where D_{50A} is the median grain size of the bed-surface material) suggests this as a minimum DEM size for grain-scale roughness analysis. We further find that the DEM grid spacing should be 1 mm or below, in order to adequately capture grain roughness, as coarser resolutions failed to detect particle imbrication. Finally, variability in roughness parameters was evident due to the natural spatial variation in gravel-bed microtopography, suggesting using a single roughness parameter is not appropriate to holistically describe the roughness of a gravel patch.

Key Words

Grain-roughness; DEM; parameterisation; close-range photogrammetry

Introduction

Calls to re-evaluate the term for roughness and improve parameterisation in future research have been made (Lane, 2005; Rice et al., 2014; Martinez-Agirre et al., 2016), due to the term being used frequently, albeit with little definition (Morvan et al., 2008; Jia and Hu, 2015).

Surface roughness in fluvial environments such as gravel-bed rivers influences the dynamic interactions between flow, sediment transport and ecology (Aberle and Nikora, 2006; Hodge et al., 2009a; Baewert et al., 2014; Curran and Waters, 2014). Previous parameterisation of roughness included subjective estimations of coefficients or the use of roughness heights based on grain size and velocity profiles (Wilcock, 1996, Smart et al., 2004). However there has been a recent move to obtaining quantitative roughness parameters including bed-elevation moments such as standard deviation, skewness and kurtosis determined from transects or digital elevation models (DEMs) (Aberle and Nikora, 2006).

47 Research on gravel-bed rivers now gathers information collected from ‘patch-scale’ DEMs
48 for roughness parameterisation, although studies differ in data collection (e.g., the size and
49 resolution of measurements) and analysis methods (e.g., detrending method and roughness
50 parameters used). Therefore, explicit definitions of a gravel patch and patch-scale DEMs are
51 still lacking; yet, it is understood the size and resolution of measurements should allow for
52 adequate representation of the surface character (Hodge et al., 2009a). Roughness parameters
53 are used as inputs for both hydraulic and morphodynamic models, such as for determining
54 flow resistance (Aberle and Smart, 2003; Tuijnder and Ribberink, 2012). Measurements of
55 bed topography (e.g., the standard deviation of bed elevations) are also helpful for obtaining
56 estimates of sediment size on the bed surface (see Pearson et al., 2017 for a review).
57 Therefore, accurate parameterisation of roughness is required to avoid error propagation in
58 several applications of fluvial science and modelling (Smart et al., 2002; Lane, 2005; Morvan
59 et al., 2008). One step towards achieving accurate roughness parameterisation is to provide
60 guidance to researchers on how to work with topographic datasets.

61 This analytical paper aims to provide insights into patch-scale gravel-bed DEM analysis for
62 obtaining roughness information. A combination of laboratory and field data is used, with the
63 application of an analytical process for fluvial gravel-bed DEMs and the consideration of an
64 extensive range of roughness parameters. Firstly, this study considers roughness spatial
65 variability.Previous research considered the small-scale spatial variability in grain size
66 (Crowder and Diplas, 1997), with applications to evaluate the effect of sampling area on the
67 accuracy of image-based grain size measurements (Graham et al. 2010), and to explain
68 spatial differences in grain entrainment (Piedra et al. 2012). We recently presented new
69 results on the spatial variability and scaling of surface structure (i.e., topography) in gravel-
70 bed rivers, allowing the isolation of roughness scales from DEMs (Bertin et al., 2017). This
71 paper continues on this emerging avenue of research, with a wider selection of roughness

parameters assessed. Secondly, this paper assesses the combined effect of DEM size and grid spacing on output roughness parameters. The current scope of literature in relation to each of these objectives is discussed in more detail in the background section following.

Background

An overview of the procedure for analytical processes considered throughout this study is provided in Figure 1. This visually presents the different analytical steps investigated, including the effect of DEM size (i.e., the spatial extent of the DEM or measured patch, Step 1) and grid spacing (equivalent to DEM resolution, Step 3). Step 1 is specific to the technique of digital photogrammetry in the generation of point clouds, but the subsequent steps are applicable to all researchers, from a broad range of disciplines, analysing topographic datasets. Complete details of the processes will be outlined in the methodology section.

DEM size

Roughness values are dependent on a suitable DEM size, as this determines the scale over which the roughness is calculated (Florinsky and Kuryakova, 2000; Smith, 2014). Research on grain roughness suggests that the size of the gravel patch measured needs to be large enough to capture a range of sediment sizes, including several large grains (Hodge et al., 2009a). However, a more quantitative guideline for the size of a DEM is required (Step 1, Figure 1), as patch-scale research has used DEM sizes ranging from 0.1 m^2 to 1 m^2 (Hodge et al., 2009a; Mao et al., 2011; Ockelford and Haynes, 2013; Rice et al., 2014). Recent literature deemed patch sizes, which equate to 21 × D_{50} in both directions, suitable for analysis of grain roughness changes for flows below entrainment threshold (Ockelford and Haynes, 2013). Unfortunately, reasons behind this decision were not presented and it is not clear if D_{50} refers to the bulk mixture or bed surface sediment, which is problematic when grain size varies greatly between surface and subsurface, such as for armoured beds.

Step 1:
Data acquisition

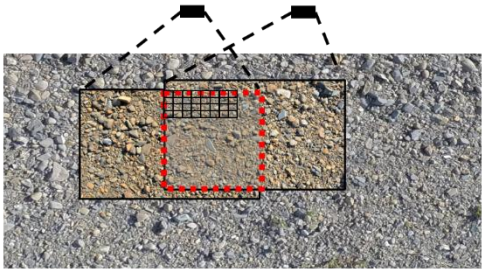

Photogrammetry; where the common field of view (CFoV) (overlap in two images) determines the patch size (red dashed line) for analysis.

Pixel size (small black squares) determined by sensor size, focal length and camera distance.

Step 2: Data processing

Stereo matching

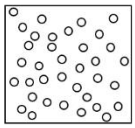

Point cloud with a resolution determined by pixel size and size determined by CFoV.

Step 3: Generation of DEM

Interpolation onto regular grid (e.g. determining grid spacing)

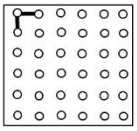

DEM maximum size (e.g. patch size) determined by CFoV and grid spacing (thick black lines) is ≥ pixel size which can be user defined.

Transect of DEM (red line) schematically depicting grain-roughness (blue dashed line).

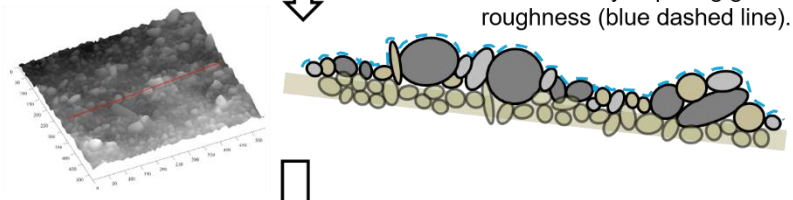

Step 4: Moving-window analysis

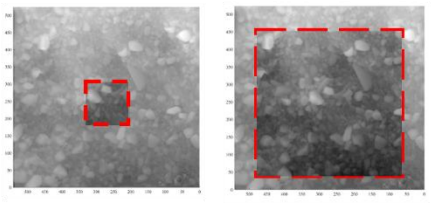

Moving-window size selection based on D_{50A} values.

Example depicts 4 x D_{50A} (left) or 16 x D_{50A} (right) in both directions.

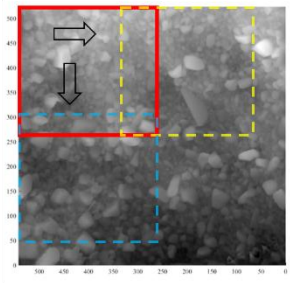

Moving window analysis with user defined window size (e.g. 10 x D_{50A} in both directions), example of 25% overlap for clarity purposes.

Black arrows indicate moving window in both directions. New windows defined with coloured dashed lines.

Step 5: Calculating roughness parameters

Roughness parameters calculated for each moving-window size (see Table I).

Figure 1. Overview diagram of the generation of topographic data using digital photogrammetry and analytical processes discussed further, including interpolation using varying grid spacingand a moving window technique.

A moving-window approach (Step 4, Figure 1) was used to determine the grain-size variability of a river reach (Crowder and Diplas, 1997), and to evaluate DEM error spatial distribution for various survey strategies and interpolation methods (Heritage et al., 2009; Milan et al., 2011). Further, studies in different applications, including large scale floodplain analysis, have altered the DEM size (using a moving window technique with a window radius ranging from 1 m to 1000 m), which allowed for the identification of threshold sizes for DEMs to produce topographic metrics (Florinsky and Kuryakova, 2000; Scown et al., 2015). These papers highlight the importance of establishing the scale of interest and using this choice to select a suitable DEM size.

Recent use of moving windows of different sizes on gravel patches distinguished roughness signatures of grains and bedforms (Bertin et al., 2017). Contrasting with grain roughness, measures of bedform roughness did not always reach stable values with window-size increases, suggesting that patch-scale DEMs may be limited in use to the analysis of grain roughness (Bertin et al., 2017, Powell et al., 2016). Just like Graham et al. (2010) using grain-size spatial variability for examining the effect of sampling area on the accuracy of grain size measurements, previous research suggests that knowledge on roughness spatial variability can provide guidance towards an appropriate DEM size for analysis of surface roughness, which will be evaluated in this study.

In reporting our experiments, we therefore use the term DEM size to refer to two things, which is worthy of clarification: (i) DEM size efers to the size of the gravel patch measured, which is a 'constant' for each patch and is presented in Table I; (ii) DEM size is then altered using moving windows, and we use our measurements of roughness spatial variability for different window sizes to identify a minimum DEM size for roughness analysis.

DEM grid spacing

Future research using high resolution data needs to consider the level of detail required for the application (Smith, 2014). For example, the grid spacing (i.e., DEM resolution) used when converting a point cloud to a DEM (Step 3, Figure 1) also determines the scale over which roughness is calculated, with previous studies stating patch-scale investigations require higher resolution and precision (Smith et al., 2012; Smith, 2014). Studies on various scales from soil properties, gravel surfaces and catchment landscapes, have found that changes in measurement resolution influence the obtained roughness values or topographic parameters and affect DEM accuracy (Zhang and Montgomery, 1994; Smith, 2014; Trevisani and Cavalli, 2016; Grieve et al., 2016; Bertin and Friedrich, 2014; Lane et al., 2000; Gao, 1998; Erskine et al., 2007; Milenković et al., 2015; Barber et al., 2016). Thus the scale of the process investigated should influence grid spacing choice

Studies on gravel beds have used grid spacing including 0.1 mm, 1 mm and 5 mm, regardless of sediment size on the patch (Buffin- Bélanger et al., 2006; Ockelford and Haynes, 2013; Hodge et al., 2009a; Bertin and Friedrich, 2014; Curran and Waters, 2014). Due to this range, it is important to investigate the effect of a resolution below, and above, the 1 mm resolution commonly used for gravel patches, in order to provide an indication to the optimal grid spacing for use in grain roughness analysis.

Methodology

Gravel-bed patches and digital elevation models (DEMs)

DEMs representing the microtopography of five gravel-bed patches from different geomorphic settings (i.e. collected from both the field and a laboratory flume) were used for the study (Figure 2).

Three DEMs collected in August 2014 from the Whakatiwai River, a small gravel-bed stream located in New Zealand North Island, and presented in Bertin and Friedrich (2016), form the field surfaces. Patches from three exposed and vegetation-free gravel bars (labelled "Field 1" to "Field 3", with numbers increasing upstream) were selected for measurements, covering a range of sediment size and surface structure (Table I). Each patch was selected at the bar head close to the water edge, for both consistency in the measurements, and ensuring the surfaces are regularly water-worked under similar hydraulic conditions.

Two armoured gravel beds called "Lab 1" and "Lab 2" formed in a non-recirculating tilting flume with glass side-walls (19 m long, 0.45 m wide and 0.5 m deep), with a flume slope set at 0.5 %, are also examined. The experimental beds were obtained from water-working two distinct sediment mixtures. A constant flow rate of 84 L/s (mean flow velocity = 0.82 m/s, shear velocity = 0.077 m/s and uniform water depth = 0.225 m) was applied until the rate of sediment transport dropped to less than 1% of the initial transport rate. Both sediment mixtures were prepared from distinct but slightly bimodal alluvial sediments (15% sand and 85% gravel, and 9% sand and 91% gravel, respectively), with size ranging from 0.7 to 35 mm (Table I). The tests were performed under condition of sediment starvation (i.e., no sediment feeding).

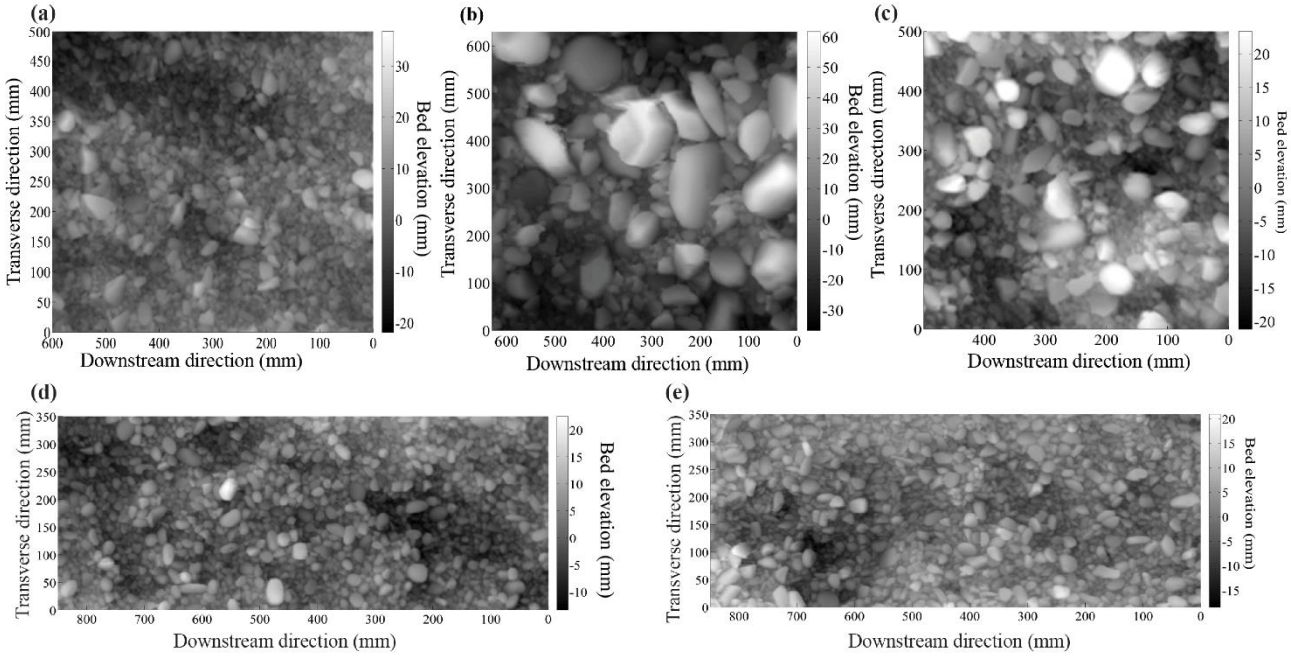

Figure 2. Digital elevation models (DEMs) displaying the gravel-bed surfaces around the mean bed level, after flat-surface detrending, by removing the combined effect of bed slope and setup misalignment: (a) Field 1; (b) Field 2; (c) Field 3; (d) Lab 1 and (e) Lab 2. The surface forming flow direction is right to left.

To allow the accurate measurement of the bed-surface topography and grain structure with digital photogrammetry for the five patches, a pair of Nikon D5100 cameras (16.4 Mpixel, 23.6 x 15.6 mm^2 sensor size) with Nikkor 20 mm lenses, was installed in stereo (horizontal baseline distance between cameras between 0.25 and 0.3 m) vertically (i.e., both cameras looking down, minimising occluded points which cannot be seen in one or the two images) above the gravel beds. Presently, a variety of image-based DEM reconstruction techniques are available, from the now conventional digital stereo (i.e. two-camera) photogrammetry, using either commercial or non-proprietary calibration and stereo-matching engines, to novel structure-from-motion (SfM) or multi-view stereo (MVS) photogrammetry (James and Robson, 2012; Fonstad et al., 2013; Javernick et al., 2014) which does not need calibration. However, a current drawback of SfM/MVS that may cause problems in recording a gravel

patch at fine scales is the likely presence of large non-linear distortions in the DEMs, due to inadequate lens distortion calibration (Fonstad et al., 2013; Ouédraogo et al., 2014), an issue that has been resolved in traditional stereo photogrammetry (Wackrow and Chandler, 2008; Bertin et al., 2015). Furthermore, as James and Robson (2012) show in their 3D measurement of a volcanic bomb (surface ~0.008 m^2), a large number of photographs (~200, of which ~90 were processed for DEM reconstruction) are required to obtain a DEM with density comparable to the DEMs obtained in the present study, which requires only two photographs. The processing time to obtain one fine-scale DEM with SfM/MVS (12 hours) is thus very long compared to the 15 minutes (stereo matching time) required by our approach.

The photogrammetric technique employed herein to obtain DEMs from stereo photographs (i.e., two overlapping images as shown in Step 1, Figure 1) consists of (i) in-situ calibration, using the method of Zhang (2000), included in Bouguet's (2010) open-access calibration toolbox for Matlab®, which requires several stereo photographs of a planar chequerboard to be recorded to determine both intrinsic (i.e., camera) and extrinsic (i.e., setup) calibration parameters; (ii) using the calibration data to accurately rectify (mean rectification error < 0.5 pixel and maximum error < 1 pixel throughout the imaging area) stereo photographs of the gravel beds to epipolar geometry, whereby corresponding pixels between overlapping images are ideally on a same scanline (i.e., corresponding pixels have the same y-coordinate); (iii) scanline-based pixel-to-pixel stereo matching using Gimel'farb's (2002) symmetric dynamic programming stereo (SDPS) algorithm, providing both point cloud data and ortho-images (Step 2, Figure 1). Using the SDPS, occluded points are interpolated based on the assumption of a continuous surface, leaving no voids. The careful design of the measurement setup (e.g., adjusting the baseline and the camera height to the relief of the surface) helps to minimise occlusions (Lane et al., 2000; Bertin et al., 2015); yet determining the proportion of occluded points is not possible. To fulfil analytical requirements of regularly-spaced data (e.g., to

measure bed-elevation structure functions) and to avoid bias introduced by non-uniform data when calculating the standard deviation of bed elevation σ_z (Hodge et al., 2009a), point clouds were interpolated (using the triangle interpolation method in Matlab) onto regular grids (i.e., raster DEMs as shown in Step 3, Figure 1) with spacing 1 mm (the reference grid spacing against which other grids are compared, see Section 3). Each DEM underwent rigorous quality assurance testing (readers can refer to Bertin et al., (2015) and Bertin and Friedrich (2016) where detailed evaluations of the laboratory and the field DEMs are presented, respectively), to ensure surface metrics derived from the DEMs had minimum effect due to DEM errors. Outliers, which accounted for less than 1% of the DEM points, were identified using the mean elevation difference parameter by comparing each DEM point with its direct neighbours (Hodge et al., 2009b), and replaced using bi-cubic spline interpolation. All DEMs were finally normalised to have a mean bed level equal to zero, and rotated to be aligned with the surface-forming flow direction. Whilst flow direction identification is straightforward for laboratory surfaces, the flow direction for field data was determined by eye from observations of channel shape and grain imbrication (Laronne and Carson, 1976; Millane et al., 2006; Bertin and Friedrich, 2016). Finally, using a least-squares fit, flat-surface detrending was undertaken to remove the influence of both the bed slope and experimental setup misalignments from the DEMs (e.g., Aberle and Nikora, 2006; Bertin and Friedrich, 2016).

As shown in Table I, camera height could not be set constant throughout both the field and the laboratory applications. The DEM characteristics therefore varied slightly between applications; although DEM resolution and vertical error remained small compared to sediment size (cf. Table I), a precondition for grain roughness characterisation (Hodge et al., 2009b). One can note that the laboratory DEMs have larger coverage, yet smaller pixel size and theoretical vertical error. This is because the laboratory DEMs were obtained by merging

three smaller overlapping DEMs, allowing shorter camera distance. We note that other measurement techniques such as laser scanning (Hodge et al., 2009a, 2009b; Aberle and Nikora, 2006) have been used by others to produce gravel-bed DEMs similar to the ones used in this study.

Table I. Summary of the GSD information (both surface and subsurface where applicable) and DEM characteristics, for the five gravel-bed patches. The subscript 'A' indicates surface sediment from the armour layer, rather than the bulk sediment. The best DEM horizontal resolution is the average pixel size on the gravel beds, which is also the average point spacing in point clouds. The theoretical vertical error is estimated using classical photogrammetric equations and depends on camera and lens specifications (i.e., sensor size, number of pixels and focal length), as well as setup characteristics (i.e., baseline and camera distance). True DEM accuracy (here the mean unsigned error) was estimated using a 3D-printed gravel-bed model to be 0.43 mm and 0.67 mm in the laboratory and the field, respectively (cf. Bertin and Friedrich, 2016).

	FIELD 1	**FIELD 2**	**FIELD 3**	**LAB 1**	**LAB 2**
D_{50} (mm)	N.A.	N.A.	N.A.	8.4	9.2
$\sigma_G = \sqrt{D_{84}/D_{16}}$	N.A.	N.A.	N.A.	3.0	2.6
D_{50A} (mm)	18.7	47.2	19.4	18.9	18.5
D_{90A} (mm)	27.3	104.7	47.7	27.1	28.1
$\sigma_{GA} = \sqrt{D_{84A}/D_{16A}}$	1.4	2.2	2.3	1.4	1.4
Patch size (mm) (downstream × transverse)	600 × 500	630 × 630	500 × 500	850 × 350	850 × 350

Normalised patch size by D_{50A} (downstream x transverse)	32 x 26	13 x 13	25 x 25	45 x 18	45 x 18
Best DEM horizontal resolution (mm)	0.20	0.22	0.19	0.17	0.16
Theoretical vertical error (mm)	0.55	0.59	0.47	0.36	0.36
Approximate camera distance (mm)	825	860	765	675	670

Grain-size distributions (GSDs)

To complement topographic information derived from DEMs and to allow comparison with sediment size, the bed-surface composition based on the sediment grains' intermediate axis was determined for each gravel patch using a single vertical photograph (number of detected grains > 400) and the image-analysis tool Basegrain®. The latter allows for automatic grain separation in digital images of gravel beds and applies the Fehr's (1987) line-sampling method for results' analysis (Detert and Weitbrecht, 2012). Independent measurements were obtained by measuring surface sediment along lines with a digital calliper (with results presented in Stähly et al., (2017)), which allowed us to calibrate the results obtained with Basegrain.

In addition to surface composition determined with Basegrain, the experimental sediment mixtures used in the laboratory were sieved to determine the sediment grading curves (Table I), particle shape and specific gravity. To distinguish GSDs of the bed surface from those of the bulk mixtures, percentiles derived from GSDs were indexed with "A" to represent characteristics of the armoured surface.

Grid spacing and the effect of DEM horizontal resolution

To quantify the effect of DEM resolution or grid spacing on the roughness information derived, point clouds of the five patches were transformed into DEMs of varying resolution by interpolating the raw elevation data (using triangle interpolation in Matlab) from point clouds on regular grids (Step 3, Figure 1) with spacing: 0.35 mm, 0.5 mm, 1 mm (the reference grid spacing), 3 mm, 10 mm, D_{50A} and 2 × D_{50A} (i.e., spacing equal to the surface median grain size and two times the surface median grain size, respectively). The decision on the grid spacings used herein was guided by grid spacings used in the literature (as presented in the background section), as well as to enable investigation of a threshold grid size decoupled from sediment size (here D_{50A}, as this is the property most commonly reported). .

Surface metrics and the moving-window analysis

To quantify the character and surface variability of the five patches, six surface metrics (see Table II) were calculated for each DEM within moving windows of different sizes. In reporting our results on moving windows, we distinguish the term DEM size from the size of the gravel patch measured (Table I); in that DEM size is varied by adjusting the size of the moving windows. The maximum window size tested is necessarily less than the patch size.

Square windows were used (in comparison to circular windows as in Scown et al., 2015), since recorded DEMs are more often square (or rectangular) in shape. The effect of the

276 measurement orientation (in the case of rectangular DEMs) was also examined. For this, the
277 initially square windows were halved either horizontally or vertically to form rectangular
278 windows with their long axis aligned either parallel or perpendicular to the flow direction. To
279 facilitate observations from the graphs and to allow comparison between the five patches
280 studied, window size in both directions was normalised by D_{50A} (i.e., calculations were made
281 within windows with an area proportional to the area covered by the surface D_{50A} determined
282 over the whole DEM). Surface metrics were obtained for each window of the designated size,
283 whilst windows are moved across the whole surface of the DEM (Step 4, Figure 1), with the
284 number of windows fitting into the DEM ranging from >2000 (at small window sizes) to <50
285 (at larger window sizes). An overlap between moving windows of 95% of the window size
286 was used, except for calculating structure functions, for which a 25% overlap was used due to
287 the very large computational demand (still, a typical run time was 24 hours per DEM).
288 Sensitivity analysis of the effect of changing the overlap size to 25% showed no adverse
289 effect interpreting the findings. However, a 95% overlap was preferred when possible due to
290 refined visual presentations of the results across window sizes (i.e., smoother graphical lines).

291 The commonly used surface metrics calculated from bed-elevations used in this study are
292 presented in Table II. Bed-elevation distribution moments contained in probability
293 distribution functions (PDFs) include σ_z, S_K and K_u and are classic descriptors of bed
294 roughness used in a number of studies at scales ranging from grain size to channel shape
295 (e.g., Aberle and Nikora, 2006; Scown et al., 2015). Surface variability about the mean
296 elevation within an area is indicated by σ_z (Eqn. 2) and represents a characteristic vertical
297 roughness scale of the bed surface, which can be used as a grain-roughness parameter in flow
298 resistance equations (Aberle and Smart, 2003; Noss and Lorke, 2016). Skewness (S_K, Eqn. 3)
299 describes the degree of asymmetry of the PDF and can be used to assess the general shape of
300 the bed surface. In this regard for water-worked gravel beds, a positive skewness is attributed

to finer grains filling depressions and reducing the magnitudes of surface deviations below mean bed level (Aberle and Nikora, 2006). Kurtosis (K_u, Eqn. 4) provides a measure of the regularity or intermittency of the bed. A distribution characterised by heavy tails and a narrow peak has a large kurtosis, with more of the variance due to infrequent extreme deviations. More uniform and compact distributions, of frequent modestly sized deviations from the mean, are of lower kurtosis values (Coleman et al., 2011).

Table II. Surface metrics calculated from gravel-bed elevations used in this study.

Parameter	Formula	Equation
Standard deviation (σ_z)	$\sigma_z^{\,2} = \frac{1}{N'}\sum_{i=1}^{N'}(Z_i - \langle Z_i \rangle)^2$	(2)
Skewness (S_K)	$S_k = \frac{1}{N'\sigma_z^{\,3}}\sum_{i=1}^{N'}(Z_i - \langle Z_i \rangle)^3$	(3)
Kurtosis (K_u)	$K_u = \left[\frac{1}{N'\sigma_z^{\,4}}\sum_{i=1}^{N'}(Z_i - \langle Z_i \rangle)^4\right] - 3$	(4)
Structure function (D_{G2})	$D_{G2}(\Delta x, \Delta y) = \frac{1}{(N-n)(M-m)}\sum_{i=0}^{N-n}\sum_{j=0}^{M-m}\{\lvert z(x_i + n\delta x, y_j + m\delta y) - z(x_i, y_j)\rvert\}^2$	(5)
Inclination index ($I0$)	$I0 = \frac{n_+ - n_-}{Ns}$	(6)

z represents the bed elevation at location (x,y) in a DEM, N' is the total number of DEM points and < > represents the mean value. $\Delta x = n\delta x$ and $\Delta y = m\delta y$; δx and δy are the sampling intervals (i.e., DEM resolution) in the longitudinal and transverse directions respectively;

311 n=1,2,3,…N and m=1,2,3,…M. N and M are the number of DEM points in the same two
312 directions. n_+ and n_- are the number of positive and negative slopes between successive DEM
313 points, respectively, and Ns is the total number of slopes.

314 Horizontal roughness lengths in both the streamwise and the cross-stream direction (L_x and
315 L_y, respectively) are scaling characteristics of a surface and are calculated from second-order
316 structure functions (Eqn. 5).

317 Structure functions, which are different from semivariograms by a factor two, measure
318 changes in elevation correlations at different spatial lags and in different directions (Figure
319 3). Small structure function values represent regions characterised by similar elevations
320 (because of DEM points located on a same grain or bedform), while large values identify
321 regions on a surface that are not correlated anymore. A gravel-bed elevation structure
322 function has three regions: a scaling region with uniform slope at small lags, a saturation
323 region at large lags, where the slope is zero, with a transition region in between, where the
324 slope decreases (Nikora et al., 1998; Hodge et al., 2009a). As shown in Figure 3, the scaling
325 region of the 1D structure function fitted with a power law, provides information about the
326 horizontal roughness lengths L_x and L_y, which are determined from the slope breakpoint,
327 located at the intersection between the tangent to the scaling region slope and the saturation
328 level asymptote, in both x and y directions (Nikora et al., 1998). Hence, L_x and L_y were
329 calculated from 1D structure functions whereby $\Delta x = 0$ and $\Delta y = 0$, respectively. The
330 maximum spatial lag to calculate D_{G2} (Eqn. 5) in both x and y directions was chosen as half
331 the window size in the same two directions, and L_x and L_y were determined at the condition
332 the saturation region was attained for all moving windows of the same size.

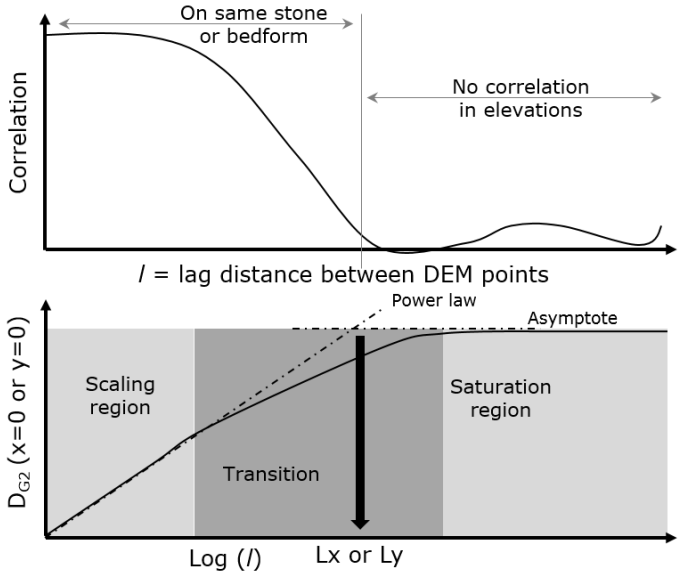

Figure 3. Typical gravel-bed elevation correlation and structure function graph for different spatial lags, used to determine horizontal roughness lengths *Lx* and *Ly*. Adapted from Smart et al. (2002).

The inclination index (*I0)* in the flow direction is calculated using Eqn. 6 (Smart et al. 2004). It analyses the signs of elevation changes between successive pairs of DEM points on transects aligned with the flow direction at a lag distance equal to the DEM resolution, where a positive slope refers to increasing bed elevations downstream. Slopes whose absolute value is below 0.01 were deemed not reliable (i.e., neither positive nor negative), and were therefore not counted in the numerator of Eqn. 6 (Millane et al., 2006). A positive inclination index reflects the dominance of positive slopes and thus particle imbrication, generally maximum in the flow direction, minimum in the direction opposite to the flow, and approximately zero in a direction transverse to the flow (Laronne and Carson, 1976; Millane et al., 2006). Characterising grain imbrication is therefore relevant for determining flow direction from bed-surface analysis, but also provides insights on bed stability and the history of the flow that shaped the surface.

The surface variability for the six surface metrics was also quantified with the coefficient of variation (CV), calculated as the standard deviation of the property determined over all moving windows divided by the mean, and expressed as a percentage. To study the effect of measurement scale on surface variability, CV was calculated for different window sizes.

Results

Because the respective effects of DEM size and grid spacing on roughness parameters cannot be presented collectively, examination is undertaken step-by-step. We start with the effect of DEM size and first examine the spatial variability of roughness parameters using moving windows. Only window size is altered during this first part of the analysis, while generic grid spacing is maintained (i.e., grid spacing equal to the reference value of 1 mm).

Roughness Spatial Variability

Figure 4 presents the coefficient of variation (CV) for all roughness parameters and gravel patches considered in this paper with changes in moving-window size. As is common practice, CV was used at the condition of positive property values only. Here, the surface metrics S_K and *I0* sometimes adopt negative values when calculated over small window sizes, whilst positive values (characteristic of a water-worked and imbricated gravel bed) are measured for all patches at larger window sizes. Therefore, calculation of CV for S_K and *I0* required adjustments in the range of window sizes, as shown. Despite this caveat, two observations can be obtained from Figure 4. Firstly, there are differences in the spatial variability of certain roughness parameters. Particularly evident are the higher CV values at a given window size, in both skewness and inclination index, an indication that these two parameters vary widely spatially within a gravel patch. Across all DEMs, the parameters which provided the lowest CV values (reaching a minimum of below 5%), were horizontal roughness lengths L_x and L_y, along with σ_z (Figure 4). Secondly, spatial variability for the

majority of roughness parameters declines with increases in moving-window size, until it plateaus out. This observation suggests the existence of a threshold DEM size, evaluated hereinafter, above which the surface roughness of the patch is characterised by the parameters and decision on the location of the DEM within the patch is becoming less important (Scown et al., 2016).

For the rest of the analysis, not all roughness parameters are presented, but instead horizontal roughness lengths, σ_z, and *I0* are chosen to exemplify trends representative of all roughness parameters. The selection comprises roughness parameters commonly used for gravel beds and as shown in Figure 4, encompasses parameters with a wide range of spatial variability, therefore maximising the representativeness of the findings.

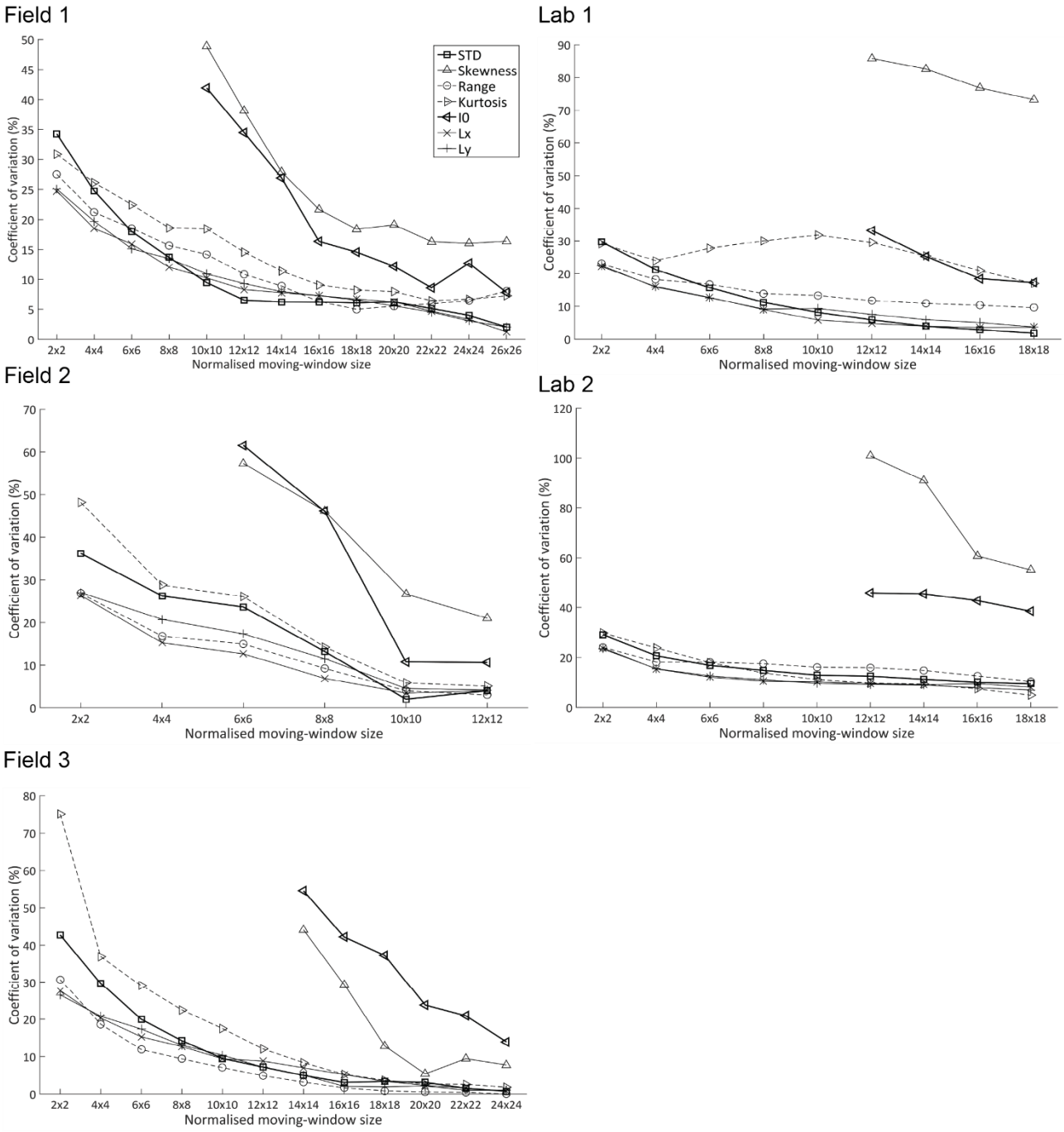

Figure 4. Coefficient of variation (CV) for all roughness parameters, for all datasets (Field DEMs left column, Lab DEMs occupy the right column), calculated at different moving-window sizes normalised in both directions by $D_{50A.}$.

Effects of DEM size and Orientation on Roughness Parameterisation

Figure 5 displays the coefficient of variation (CV) in σ_z for all five datasets. Previously, we observed a consistent decrease in spatial variability with window size increases for all

roughness parameters studied (Figure 4). Focusing on one parameter now enables examination of whether a threshold DEM size represented by a plateau in variability exists, as well as to examine the effect of patch orientation.

Figure 5 confirms a clear effect of window (hence DEM) size on the roughness statistics, for all patches. The smaller the moving-window size, the larger the variance in results produced across the patch. Variance reduces and plateaus as the window size increases, between 12 and 18 × D_{50A} across the majority of the patches. However, there are patches showing a further decrease in variance following this observed plateau (Figures 5a and 5c). Given bedforms were not filtered from DEMs for this analysis; we believe this observation suggests two spatial scales of surface roughness present.

Across all patches the size of the window (hence DEM size) has a greater control on roughness statistics than the orientation of the window. Similarities in statistics exist regardless of the orientation (shape) of the window, apart from Field 2 (Figure 5b), where vertical windows result in lower CV, and Lab 1 (Figure 5d), where CV is higher for vertical windows and lower for horizontal windows compared to the use of square windows. These differences suggest surface anisotropy in the flow direction for Lab 1, whilst Field 2 is characterised by higher variability in σ_z in the transverse direction.

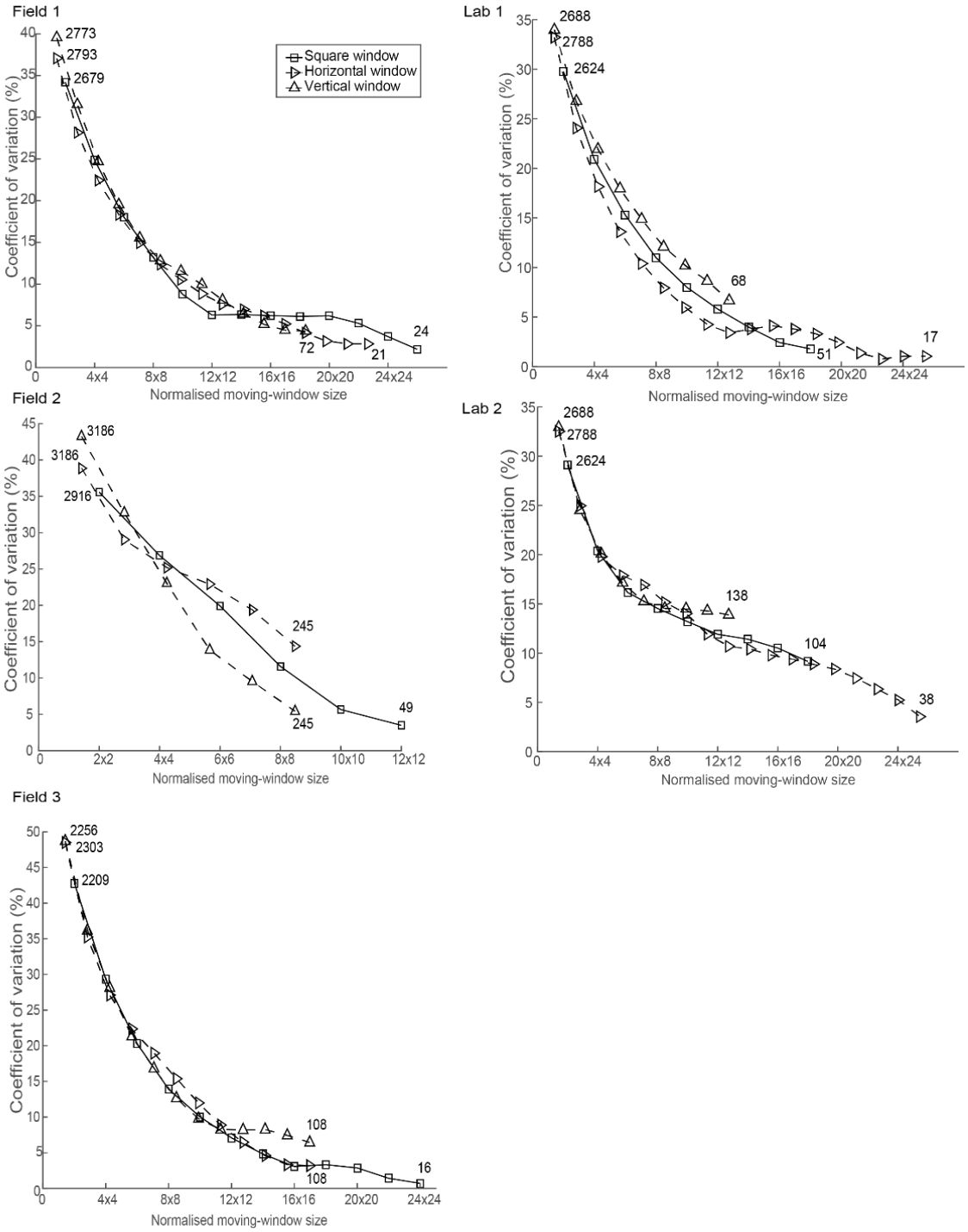

Figure 5. Coefficient of variation (CV) in σ_z for all datasets (Field DEMs left column, Lab DEMs occupy the right column), calculated at different moving-window sizes normalised in both directions by $D_{50A.}$ The number of windows generated for the maximum and minimum sizes are provided on the graphs.

Boxplots obtained using the moving-window analysis technique are presented in Figure 6, for σ_z, which demonstrate trends that are apparent across roughness parameters (Figure 4). Supplementing the analysis of roughness spatial variability using CV (Figures 4 and 5), boxplots enable examination of the evolution of the median value of a roughness parameter with window size increases. For roughness statistics calculated at small window sizes, the variability was larger than that at larger window sizes (Figure 6), which echoes previous observations using CV (Figures 4 and 5). Visually both the median values and the variability in statistics (e.g., boxplot whiskers) plateau between 14 -18 × D_{50A} for all patches (Figure 6). These plateaus were confirmed statistically using 95% confidence intervals and a paired t-test. The plateaus indicate the window (hence DEM) size is adequately detecting the topographic information under the scale of interest. Figures 5 and 6 suggest once the DEM size exceeds between 16-18 × D_{50A} in both directions in the field DEMs, and smaller sizes between 14-16 × D_{50A} in the laboratory, information derived from DEMs is deemed to provide a suitable indication of the overall surface roughness with little effect due tosurface variability. Noticeably, Field 2 (Figures 5b and 6b) began to plateau at smaller window sizes (10-12 × D_{50A}) than the other two field DEMs. However, Field 2 was the patch examined with the coarsest sediment and the smallest normalised patch size (Table I), which may impede effective plateau identification.

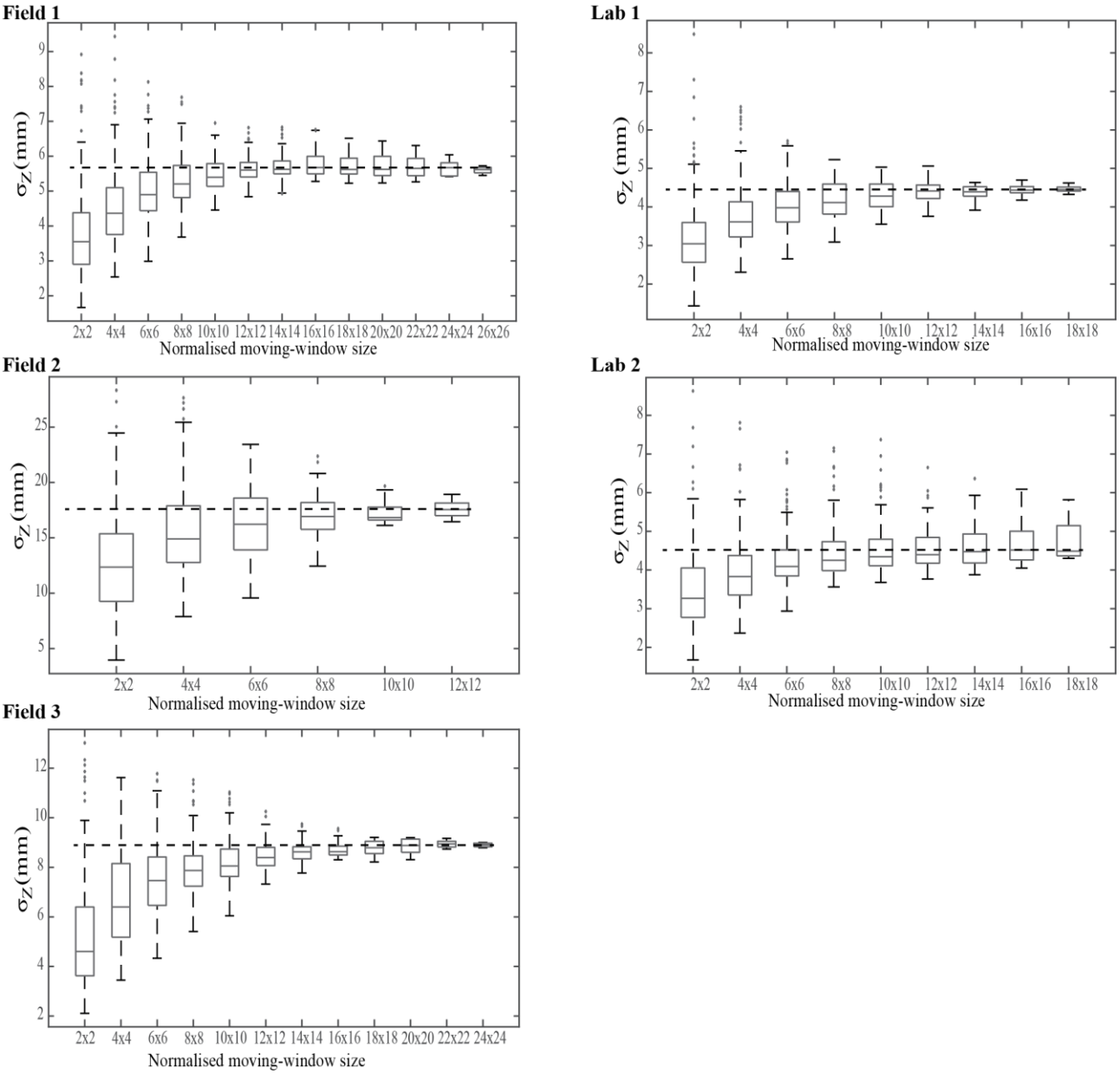

Figure 6. Standard deviation of bed elevations (σ_z) for all datasets, (Field DEMs left column, Lab DEMs occupy the right column), calculated at different moving-window sizes normalised in both directions by $D_{50A.}$ Horizontal line in the boxplot represents the median value for each DEM size and whiskers display the variability in results. Dashed lines were added to help visualise the plateauing in σ_z with window size increases.

Effects of Grid spacing on Roughness Parameterisation

Figure 7 presents results of varying DEM grid spacing on two roughness statistics, σ_z and *I0*, which have been chosen to reflect the patterns observed across parameters (Figure 4). For this analysis, only grid spacing was varied, whilst parameters were calculated over the complete DEM size (i.e., patch size).

Figure 7 shows minimal differences between using a 0.35 mm and a 1 mm grid spacing, which was observed across all patches. 1 mm corresponds to the size of the smallest surface grains identified in this study, which also corresponds to a ratio of between 1 to 20 and 1 to 50 when compared with D_{50A} (cf. Table I). For this reason, it is preferred presenting small grid sizes in absolute values (i.e., not normalised by D_{50A}). Figure 7a displays stable σ_z with changes to grid spacing exceeding 1 mm, up to a grid size equal to $D_{50A,}$ for all patches, apart from Field 2, which displays differences at a grid spacing equally the D_{50A} value. However, there are evident differences in inclination index (*I0*) at the coarser spacing, with grid spacing exceeding 1 mm providing fluctuating values, generally negative, and therefore unable to detect surface grain imbrication. This echoes previous observations of *I0* (and skewness) being more variable spatially within a patch than σ_z (Figure 4), and thus requires smaller grid spacing for roughness characterisation.

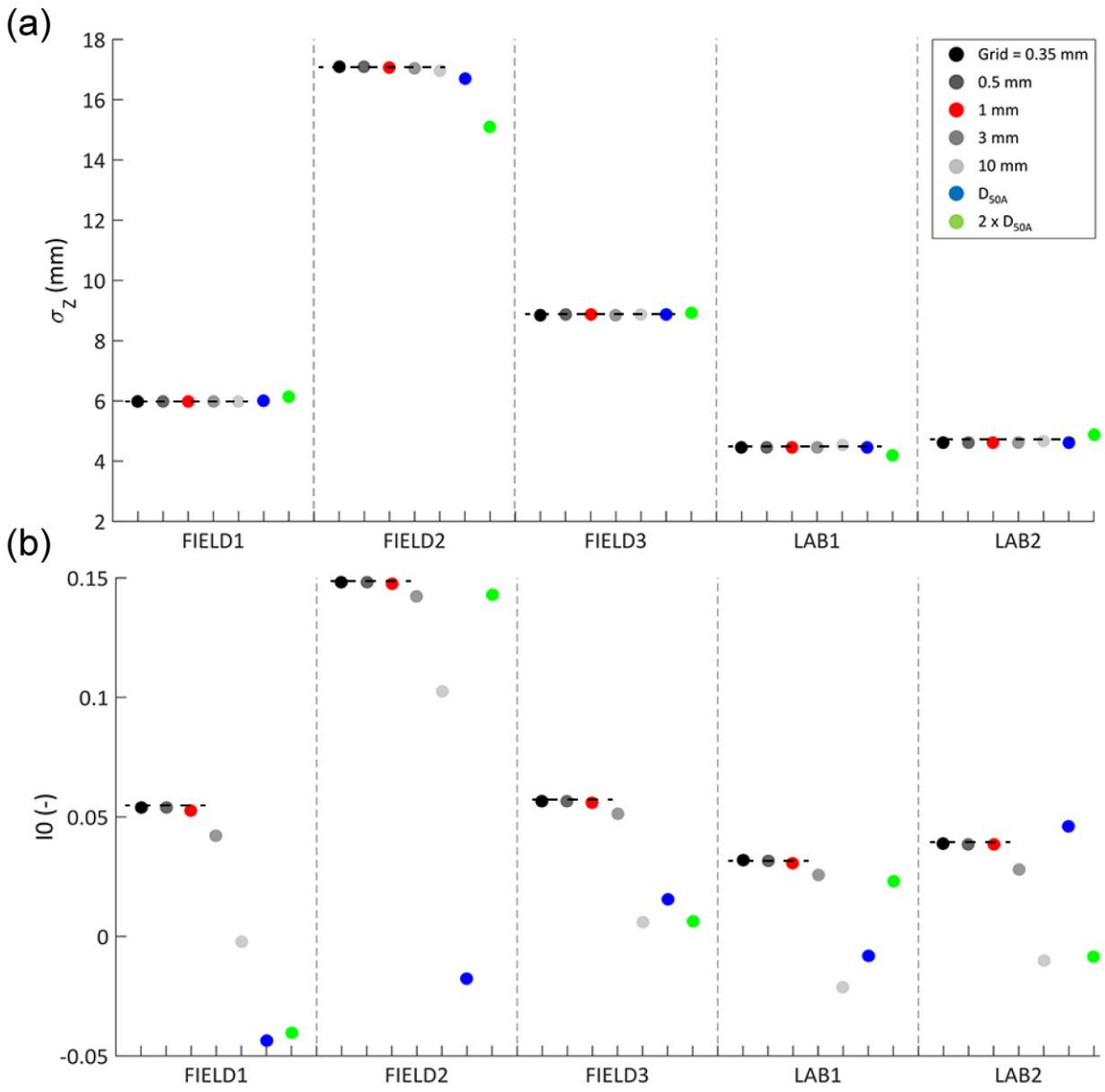

Figure 7. The effect of grid spacing for all datasets on the (a) standard deviation (σ_z) and (b) inclination index in the flow direction (*I0*). The selection of the two surface metrics was based on the consideration that σ_z and *I0* encompass the patterns observed over all parameters. Horizontal lines were added to help visualise the similarities in data points. D_{50A} values are presented in Table I.

460 **Discussion**

461 ***Surface variability and roughness parameters***

462 Previous studies using gravel-bed DEMs for roughness parameterisation often differ in terms
463 of the DEM size and grid spacing used for analysis. Common to all studies however, is the
464 assumption that parameters derived from DEMs are reliable measurements of the surface. We
465 show that accounting for spatial variability of the surface is important, as it has implicit
466 connections with analytical requirements (e.g., the required DEM size and grid spacing).

467 In this study, we have quantified spatial variability in roughness parameters to provide deeper
468 insights into the fundamentals required for DEM analysis. Novel results obtained show that
469 spatial variability in roughness parameters exists across a gravel patch, as processes shaping
470 alluvial beds naturally result in surface heterogeneity at all scales (e.g., Graham et al., 2010;
471 Nelson et al., 2014; Scown et al., 2015). This complements previous observations of spatial
472 variability in sediment size. Besides, we show that roughness parameters differ greatly on
473 their degree of spatial variability within a patch (e.g., the vertical shift between roughness
474 parameters shown in Figure 4).

475 Roughness parameters with the lowest and most consistent variance over window size
476 increases (e.g., horizontal roughness lengths and σ_z) are deemed the parameters adequate to
477 provide robust measures of roughness over a patch. However, certain roughness parameters
478 display high variance (e.g., skewness), with fluctuations in this parameter reflecting spatial
479 variability in particle arrangement (Aberle and Nikora, 2006). Similarly, large fluctuations in
480 inclination index for a given window size indicate heterogeneous grain imbrication (Figure
481 4).

482 ***DEM size***

483 Although differing in their degree of spatial variability, all roughness parameters examined
484 show a consistent reduction in spatial variability with window size increases (Figure 4). Thus,
485 one can use measurements of spatial variability to identify a suitable DEM size that ensures
486 roughness parameters independent of the surface heterogeneity (e.g., Scown et al. 2015,
487 2016). A similar approach was used by Graham et al. (2010) to determine a suitable
488 measurement size for maximising the accuracy of image-based grain size measurements.

489 Figure 5 shows a greater control of window size (hence DEM size) on roughness statistics
490 than the orientation (shape) of the window. Overall, we deem the orientation of
491 measurements to not have a clear influence on the roughness statistics, unless the surface is
492 clearly anisotropic. Therefore we suggest using square moving windows for analysis of
493 gravel bed spatial variability, in order to reduce the effect of anisotropy.

494 Our findings of a reduction in CV with increases in window size (Figures 4 and 5) are in line
495 with a field-based study of roughness length and bed shear stress in a coarse-bed channel,
496 which found reduced CV with an increase in sample size (i.e., an increased number of
497 samples collected over an increased spatial coverage) (Cienciala and Hassan, 2016). Once a
498 certain DEM size is reached, at which grain-roughness information is measured, CV may
499 reduce again due to the presence of bedforms or larger scale roughness elements (Figure 5).
500 This supports the theory of gravel patches displaying mixed-fractal behaviour with two scales
501 of roughness, whereby bedform roughness is represented by a fractal band exceeding the
502 largest grains (Robson et al., 2002; Aberle and Nikora, 2006; Bergey, 2006; Qin and Ng,
503 2012; Noss and Lorke, 2016). Although CV reduces following a plateau, gravel patches
504 display variance continually due to the lack of uniformity in the nature of a gravel-bed
505 surface. This lack of uniformity leads to topographic variability both within and between

patches analysed in this study, due to differences in sorting, packing, burial, imbrication, shape and size of the sediment (Graham et al., 2010).

The plateau in variance observed in the field DEMs occurred at larger sizes, which we believe is due to poorly sorted sediment (Table I) and the increased prevalence of small-scale bedforms in the field (seen in Figure 2). Bedforms can contribute to an increased surface complexity in comparison to the more uniform laboratory DEMs, with variance plateauing at smaller sizes (Bertin and Friedrich, 2016).

As mentioned previously, plateaus were observed when the median values become stable and variability remains consistent as window size increases further (Figures 5 and 6). These observed plateaus were confirmed statistically, using 95% confidence intervals to assess variability (also used in work by Cienciala and Hassan (2016) to assess spatial variability in data relating to sample size) and a paired t-test to assess for statistical differences between mean values for the data at each moving-window size. The statistical confirmation used both methods, as in some parameters the median values plateaued, however variability fluctuated, and observed thresholds considered both of these factors to be stable for estimation of an appropriate DEM size. Therefore, in certain roughness parameters, such as skewness and σ_z in Field 2, a plateau was not observed, possibly due to a small DEM size compared to D_{50A} and high spatial variability across the surface.

Grid spacing

A previous study by Scown et al. (2015), investigating the effect of DEM size on floodplain topography did not consider the effect of grid spacing on the outputs. In contrast, we find grid spacing to have an effect on roughness statistics (Figure 7).

The lack of differences between 0.35 mm and 1 mm grid spacing for all roughness parameters measured in this study (Figure 7), suggests these grid spacings are adequately

capturing the grain roughness for a range of sediment size (D_{50A} = [19 - 47 mm]) (Hodge et al., 2009a; Hodge et al., 2009b). Throughout our DEM size analysis a grid spacing of 1 mm was used, as this is already degraded from a point spacing of ~0.2 mm in point clouds (Table I) and provided the best DEM quality results we could obtain, with reasonable efficiency. Furthermore, this is the grid spacing that other researchers have used (Hodge et al., 2009a; Curran and Waters, 2014; Bertin et al., 2017).

Exceeding the 1 mm grid spacing affects the results, suggesting using these resolutions do not provide suitable grain-roughness statistics and even induce errors (Milenković et al., 2015). The differences in values observed at these grid spacings is due to complex surface topography being lost, or the spatial variability of the surface being non-identifiable (Buffin- Bélanger et al., 2006; Hodge et al., 2009a). Previous studies have found that using a coarser grid spacing of 5 mm prevented the identification of the spatial variability of a sediment surface (Buffin- Bélanger et al., 2006). For example, coarser grid spacing may pick up bedform roughness, reflecting the variability between humps and hollows of bedforms, and warping the grain-scale statistics. These differences at larger grid spacing are particularly evident in inclination index (Figure 7b) with values of 0 or negative, which indicates there is no imbrication of sediment grains. This suggests larger grid spacing does not identify grain imbrications that are observed for resolutions below 3 mm.

Implications of the research

Measurement of roughness spatial variability to explain surface processes

Assessing spatial variability of a gravel-bed surface is of importance to studies investigating the interactions between sediment and flow, for instance to explain measured spatial differences in sediment transport (Haschenburger and Wilcock, 2003; Casas et al., 2010). Using patch-scale DEMs and a moving-window technique, we were able to show that using

554 parameters such as σ_z and roughness lengths from structure functions, although provide stable
555 measures of roughness, may be inappropriate for spatial-variability characterisation. In
556 particular, Figure 4 has highlighted the need to holistically represent roughness using a range
557 of roughness parameters, such as those presented in this study, to gain an understanding of
558 the surface roughness and its spatial variability. This implication provides a step towards the
559 improvement to the calculation of flow resistance equations, which formerly used subjective
560 roughness coefficients, resulting in errors (Powell 2014). Contrasting with σ_z, we show that
561 grain imbrication and bed-elevation skewness vary greatly within a patch (Figure 4), which
562 has important implications when deciding which bed parameters to measure to explain
563 process heterogeneity, such as sediment transport.

564 ***Suitable DEM size for grain-roughness characterisation***

565 We suggest that a DEM size exceeding 16 × D_{50A} in both directions (which is the modal
566 plateau value from all roughness parameters and DEMs) is required to provide reliable grain-
567 roughness statistics. This recommendation of DEM size is supported by our previous work
568 (Bertin et al., 2017, Figures 2 and 6), whereby the analysis of roughness spatial variability
569 was extended to 35 DEMs and included DEMs collected in a laboratory flume by Aberle and
570 Nikora (2006) and the Waimakariri River (Smart et al, 2004).

571 At first look, the plateaus obtained appear lower than the value of 21 × D_{50} deemed
572 appropriate for patch size in previous literature (Ockelford and Haynes, 2013). A possible
573 reason is that sediment size in our study is based on the armour (i.e., surface) layer, whilst we
574 believe Ockelford and Haynes (2013) refer to the subsurface (or bulk mixture) D_{50} (based on
575 D_{50} of 4.8 mm). To allow comparison, the thresholds obtained here need to be converted from
576 only considering the armour layer, to the subsurface layer too. Assuming an armouring ratio
577 of 2 (i.e. $D_{50A}/D_{50} = 2$), which has been measured for our experimental beds (cf. Table I) and

observed in gravel-bed rivers in the field (Oldmeadow and Church, 2006), the thresholds in this paper would be between 28-36 × D_{50}. Therefore these thresholds are actually higher than the 21 × D_{50} suggested by Ockelford and Haynes (2013) and our results stress the importance of sediment sorting and bedform prevalence (i.e., spatial organisation) on these thresholds. Further, we believe this highlights the importance of a required uniformity within research for data analysis procedures in order to facilitate comparisons between studies. This statement supports a view in larger-scale studies, which, in order to delineate different features and scales of roughness across a floodplain, have stated that research requires an automated process to extract quantitative data from data of varying quality (Bertoldi et al. 2012). Recommendations such as those presented here are a step towards achieving this.

Similar to this patch-scale work, Scown et al. (2016) found spatial organisation of a surface and DEM size to influence measurements of floodplain topography and analytical requirements. The fact that the same findings have been observed at two vastly different spatial scales of fluvial surfaces (i.e., from mm to km) is further evidence of a continuum of roughness scales in the environment. Both studies also support the idea that analysis of roughness spatial variability is effective in detecting transitions between scales, which is an avenue of research that could benefit from further exploration.

Suitable grid spacing for grain-roughness characterisation

Our finding that grid spacing exceeding 1 mm is not able to identify grain imbrication has implications for the collection of high-resolution topographic data. For the goal of grain-roughness parameterisation, it is important to obtain a resolution which can adequately detect individual grains, yet with the ability to be efficiently computated (e.g., use of a 1 mm grid spacing rather than 0.2 mm in this study). Therefore the researcher should make a decision in regards to computation time, and a compromise made between using a sufficient grid size

(e.g., 1 mm) and data quality desired. A major benefit of high resolution data is that the data can be resampled at differing spacing required by the analysis (Ockelford and Haynes, 2013). Future work could explore the effect of grid spacing on larger patches than those presented here (as well as at floodplain scale, which was not formerly conducted), and determine requirements for analysing bedform roughness.

Conclusions

In this study, we used an analytical process based on roughness spatial variability, aimed to improve our understanding of how to analyse topographic data for gravel-bed roughness parameterisation, which is of increasing relevance for fluvial research. We have found that the scale of roughness under investigation is a vital pre-analysis decision required by the researcher, as the surface morphology and structure can influence the analysis required for a DEM. The study focused on grain-roughness characterisation using gravel-patch DEMs.

Firstly, spatial variability in microtopography across a gravel-bed was adequately quantified using the moving-window analysis technique. This evident variability suggests that one single roughness parameter, such as standard deviation, is not sufficient to represent grain-scale roughness; therefore using a combination of roughness parameters, as presented in this study, provides a more holistic view of surface complexity.

Secondly, the size of DEM influences the calculated roughness statistics, with a plateau in variance observed between 16-18 × D_{50A} in the field DEMs, and between 14-16 × D_{50A} in the laboratory, suggesting these DEM sizes provide robust measures of surface roughness. Differences in the effect of DEM size between laboratory and field were found to be due to multiple scales of roughness present on a gravel surface and differing sediment sorting.

Minimal differences between grid spacing below 1 mm indicate that the same quality results can be obtained at less computation time, using the coarser grid spacing. However, it is

essential for researchers to consider the scale of investigation, as using coarser resolutions will cause a loss of topographic information and inadequately represent grain roughness, rather focusing on roughness of larger scales, such as bedform roughness. This was particularly apparent when quantifying grain imbrication, which failed for grid spacings exceeding 1 mm.

Based on this study, which considered patches of varying sediment size, surface morphology and from different environments, we suggest for grain-scale roughness research using a DEM size and therefore patch size exceeding $16 \times D_{50A}$ in both directions and using a grid spacing of 1 mm or below. As these insights come from a range of environments and sediment, we anticipate adequate roughness parameterisation in future research using guidance presented in this paper, which will also facilitate comparisons between studies.

Acknowledgements:

The study was partly funded by the Marsden Fund (Grant No. UOA1412), administered by the Royal Society of New Zealand. The authors would like to thank anonymous reviewers whose constructive comments helped to improve the manuscript.

References

Aberle, J., and Nikora, V., 2006. Statistical Properties of Armored Gravel Bed Surfaces. Water Resour. Res., 4211, W11414, DOI: 10.1029/WR004674

Aberle, J., and Smart, G., 2003. The Influence of Roughness Structure on Flow Resistance on Steep Slopes. Journal of Hydraulic Research, 413, 259-269.

Baewert, H., Bimböse, M., Bryk, A., Rascher, E., Schmidt, K., Morche, D., 2014. Roughness Determination of Coarse Grained Alpine River Bed Surfaces using Terrestrial Laser Scanning Data. Zeitschrift Für Geomorphologie, Supplementary Issues, 581, 81-95.

649 Barber, M. E., Grings, F. M., Álvarez-Mozos, J., Piscitelli, M., Perna, P. A., Karszenbaum,
650 H., 2016. Effects of Spatial Sampling Interval on Roughness Parameters and Microwave
651 Backscatter Over Agricultural Soil Surfaces. Remote Sensing, 86, 458.
652 Bergey, E. A., 2006. Measuring the Surface Roughness of Stream Stones. Hydrobiologia,
653 5631, 247-252.
654 Bertin, S., and Friedrich, H., 2014. Measurement of Gravel-Bed Topography: Evaluation
655 Study Applying Statistical Roughness Analysis. J. Hydraul. Eng., 1403, 269-279.
656 Bertin, S., Friedrich, H., Delmas, P., Chan, E., and Gimel'farb, G., 2015. Digital stereo
657 photogrammetry for grain-scale monitoring of fluvial surfaces: Error evaluation and
658 workflow optimisation. ISPRS Journal of Photogrammetry and Remote Sensing, 101, 193-
659 208.
660 Bertin, S., and Friedrich, H., 2016. Field Application of Close- range Digital
661 Photogrammetry CRDP for Grain- scale Fluvial Morphology Studies. Earth Surf. Process.
662 Landforms, DOI: 10.1002/esp.3906
663 Bertin, S., Groom, J. and Friedrich, H., 2017 Isolating roughness scales of gravel-bed
664 patches. Water Resour. Res., 53, 6841 - 6856. doi:10.1002/2016WR020205.
665 Bertoldi, W., Piegay, H., Buffin- Bélanger, T., Graham, D. and Rice, S. (2012) Applications
666 of Close- Range Imagery in River Research. Fluvial remote sensing for science and
667 management, 341-366.
668 Bouguet, J.-Y., 2010 Camera calibration toolbox for Matlab, Caltech, Pasadena, California.
669 Avaliable at: http://vision.caltech.edu/bouguetj/calib_doc\
670 Buffin- Bélanger, T., Rice, S., Reid, I., Lancaster, J., 2006. Spatial Heterogeneity of
671 Near- bed Hydraulics Above a Patch of River Gravel. Water Resour. Res., 424.

672 Casas, M., Lane, S., Hardy, R., Benito, G., Whiting, P., 2010. Reconstruction of
673 Subgrid- scale Topographic Variability and its Effect upon the Spatial Structure of
674 Three- dimensional River Flow. Water Resour. Res., 463.
675 Cienciala, P., and Hassan, M. A., 2016. Sampling Variability in Estimates of Flow
676 Characteristics in Coarse- bed Channels: Effects of Sample Size. Water Resour. Res., 52 ,
677 1899-1922, DOI: 10.1002/2015WR017259.
678 Coleman, S. E., Nikora, V. I., Aberle, J., 2011. Interpretation of Alluvial Beds through
679 Bed- elevation Distribution Moments. Water Resour. Res., 4711, W11505, DOI:
680 10.1029/2011WR010672
681 Crowder, D. W., and Diplas, P., 1997. Sampling Heterogeneous Deposits in Gravel-Bed
682 Streams. J. Hydraul. Eng., 12312, 1106-1117.
683 Curran, J. C., and Waters, K. A., 2014. The Importance of Bed Sediment Sand Content for
684 the Structure of a Static Armor Layer in a Gravel Bed River. Journal of Geophysical
685 Research: Earth Surface, 1197, 1484-1497.
686 Detert, M., and Weitbrecht, V., 2012. Automatic Object Detection to Analyze the Geometry
687 of Gravel Grains–a Free Stand-Alone Tool. Proceedings of River Flow 2012, 595-600.
688 Erskine, R. H., Green, T. R., Ramirez, J. A., MacDonald, L. H., 2007. Digital Elevation
689 Accuracy and Grid Cell Size: Effects on Estimated Terrain Attributes. Soil Sci. Soc. Am.
690 J., 714, 1371-1380.
691 Fehr, R., 1987. Geschiebeanalysen in Gebirgsflüssen: Umrechnung Und Vergleich Von
692 Verschiedenen Analyseverfahren, Versuchsanst. für Wasserbau, Hydrologie u.
693 Glaziologie.
694 Florinsky, I. V., and Kuryakova, G. A., 2000. Determination of Grid Size for Digital Terrain
695 Modelling in Landscape Investigations—exemplified by Soil Moisture Distribution at a
696 Micro-Scale. Int. J. Geogr. Inf. Sci., 148, 815-832.

Fonstad, M., Dietrich, J., Courville, B., Jenson, J. and Carbonneau, P., 2013 Topographic structure from motion: a new development in photogrammetric measurement. Earth Surf. Process. and Landform, 384, 421-430.

Gao, J., 1998. Impact of Sampling Intervals on the Reliability of Topographic Variables Mapped from Grid DEMs at a Micro-Scale. Int. J. Geogr. Inf. Sci., 128, 875-890.

Gimel'farb, G., 2002. Probabilistic Regularisation and Symmetry in Binocular Dynamic Programming Stereo. Pattern Recog. Lett., 234, 431-442.

Graham, D. J., Rollet, A., Piégay, H., Rice, S. P., 2010. Maximizing the Accuracy of Image- based Surface Sediment Sampling Techniques. Water Resour. Res., 462, W02508, DOI: 10.1029/2008WR006840

Grieve, S. W., Mudd, S. M., Milodowski, D. T., Clubb, F. J., Furbish, D. J., 2016. How does Grid-Resolution Modulate the Topographic Expression of Geomorphic Processes? Earth Surface Dynamics, 4, 627-653.

Haschenburger, J. K., and Wilcock, P. R., 2003. Partial Transport in a Natural Gravel Bed Channel. Water Resour. Res., 391, DOI: 10.1029/2002WR001532

Heritage, G. L., Milan, D. J., Large, A. R., Fuller, I. C., 2009. Influence of Survey Strategy and Interpolation Model on DEM Quality. Geomorphology, 1123, 334-344.

Hodge, R., Brasington, J., and Richards, K., 2009a. Analysing Laser- scanned Digital Terrain Models of Gravel Bed Surfaces: Linking Morphology to Sediment Transport Processes and Hydraulics. Sedimentology, 567, 2024-2043.

Hodge, R., Brasington, J., and Richards, K., 2009b. In Situ Characterization of Grain- scale Fluvial Morphology using Terrestrial Laser Scanning. Earth Surf. Process. Landforms, 347, 954-968.

James, M. and Robson, S., 2012 Straightforward reconstruction of 3D surfaces and topography with a camera: Accuracy and geoscience application. Journal of Geophysical Research: Earth Surface 11F3.

Javernick, L., Brasington, J. and Caruso, B., 2014 Modelling the topography of shallow braided rivers using Structure-from-Motion photogrammetry. Geomorphology, 213, 166-182.

Jia, Z., and Hu, Z., 2015. Evaluation Methods of Material Surface Macro-Roughness. Materials Research Innovations, 19, S8-293-S8-296.

Lane, S., James, T., Crowell, M., 2000. Application of Digital Photogrammetry to Complex Topography for Geomorphological Research. The Photogrammetric Record, 1695, 793-821.

Lane, S. N., 2005. Roughness–time for a Re- evaluation? Earth Surf. Process. Landforms, 302, 251-253.

Laronne, J., and Carson, M., 1976. Interrelationships between Bed Morphology and Bed- material Transport for a Small, Gravel- bed Channel. Sedimentology, 231, 67-85.

Mao, L., Cooper, J. R., Frostick, L. E., 2011. Grain Size and Topographical Differences between Static and Mobile Armour Layers. Earth Surf. Process. Landforms, 3610, 1321-1334.

Martinez-Agirre, A., Álvarez-Mozos, J., Giménez, R., 2016. Evaluation of Surface Roughness Parameters in Agricultural Soils with Different Tillage Conditions using a Laser Profile Meter. Soil Tillage Res., 161, 19-30.

Milan, D. J., Heritage, G. L., Large, A. R., Fuller, I. C., 2011. Filtering Spatial Error from DEMs: Implications for Morphological Change Estimation. Geomorphology, 1251, 160-171.

744 Milenković, M., Pfeifer, N., Glira, P., 2015. Applying Terrestrial Laser Scanning for Soil
745 Surface Roughness Assessment. Remote Sensing, 72, 2007-2045.
746 Millane, R., Weir, M., Smart, G., 2006. Automated Analysis of Imbrication and Flow
747 Direction in Alluvial Sediments using Laser-Scan Data. Journal of Sedimentary Research,
748 768, 1049-1055.
749 Morvan, H., Knight, D., Wright, N., Tang, X., Crossley, A., 2008. The Concept of Roughness
750 in Fluvial Hydraulics and its Formulation in 1D, 2D and 3D Numerical Simulation
751 Models. Journal of Hydraulic Research, 462, 191-208.
752 Nelson, P., Bellugi, D. and Dietrich, W., 2014 Delineation of river bed-surface patches by
753 clustering high-resolution spatial grain size data. Geomorphology, 205, 102-119. DOI:
754 10.1016/j.geomorph.2012.06.008
755 Nikora, V. I., Goring, D. G., Biggs, B. J., 1998. On Gravel- bed Roughness Characterization.
756 Water Resour. Res., 343, 517-527.
757 Noss, C., and Lorke, A., 2016. Roughness, Resistance, and Dispersion: Relationships in
758 Small Streams. Water Resour. Res., 524, 2802-2821.
759 Ockelford, A., and Haynes, H., 2013. The Impact of Stress History on Bed Structure. Earth
760 Surf. Process. Landforms, 387, 717-727.
761 Oldmeadow, D. F., and Church, M., 2006. A Field Experiment on Streambed Stabilization by
762 Gravel Structures. Geomorphology, 783, 335-350.
763 Pearson, E., Smith, M., Klaar, M. and Brown, L., 2017. Can high resolution 3D topographic
764 surveys provide reliable grian size estimates in gravel bed rivers? Geomorphology, 293,
765 143-155.
766 Piedra, M. M., Haynes, H., Hoey, T. B., 2012. The Spatial Distribution of Coarse Surface
767 Grains and the Stability of Gravel River Beds. Sedimentology, 593, 1014-1029.

768 Powell, D.M. (2014) Flow resistance in gravel-bed rivers: Progress in research. Earth-Science
769 Reviews 136, 301-338.
770
771 Powell, D. M., Ockelford, A., Rice, S. P., Hillier, J. K., Nguyen, T., Reid, I., Tate, N. &
772 Ackerley, D., 2016. Structural properties of mobile armors formed at different flow
773 strengths in gravel- bed rivers. Journal of Geophysical Research: Earth Surface, 1218,
774 1494-1515.
775 Qin, J., and Ng, S., 2012. Estimation of Effective Roughness for Water-Worked Gravel
776 Surfaces. J. Hydraul. Eng., 13811, 923-934.
777 Rice, S. P., Buffin- Bélanger, T., Reid, I., 2014. Sensitivity of Interfacial Hydraulics to the
778 Microtopographic Roughness of Water- lain Gravels. Earth Surf. Process. Landforms,
779 392, 184-199.
780 Robson, B., Chester, E., Barmuta, L., 2002. Using Fractal Geometry to make Rapid Field
781 Measurements of Riverbed Topography at Ecologically Useful Spatial Scales. Marine and
782 Freshwater Research, 536, 999-1003.
783 Scown, M. W., Thoms, M. C., De Jager, N. R., 2015. Measuring Floodplain Spatial Patterns
784 using Continuous Surface Metrics at Multiple Scales. Geomorphology, 245, 87-101.
785 Scown, M. W., Thoms, M.C. and De Jager, N. R., 2016 An index of floodplain surface
786 complexity. Hydrology and Earth System Sciences, 201, 431-441.
787 Smart, G., Aberle, J., Duncan, M., Walsh, J., 2004. Measurement and Analysis of Alluvial
788 Bed Roughness. Journal of Hydraulic Research, 423, 227-237.
789 Smart, G. M., Duncan, M. J., Walsh, J. M., 2002. Relatively Rough Flow Resistance
790 Equations. J. Hydraul. Eng., 1286, 568-578.
791 Smith, M., Vericat, D., Gibbins, C., 2012. Through-Water Terrestrial Laser Scanning of
792 Gravel Beds at the Patch Scale. Earth Surf. Process. Landforms, 374, 411-421.

793 Smith, M. W. 2014. Roughness in the Earth Sciences. Earth-Sci. Rev., 136, 202-225.
794 Stähly, S., Friedrich, H., & Detert, M., 2017. Size Ratio of Fluvial Grains' Intermediate Axes
795 Assessed by Image Processing and Square-Hole Sieving. Journal of Hydraulic
796 Engineering, 06017005.
797 Trevisani, S., and Cavalli, M., 2016. Topography-Based Flow-Directional Roughness:
798 Potential and Challenges. Earth Surface Dynamics, 4, 343-358.
799 Tuijnder, A. P., and Ribberink, J. S., 2012. Experimental Observation and Modelling of
800 Roughness Variation due to Supply-Limited Sediment Transport in Uni-Directional Flow.
801 Journal of Hydraulic Research, 505, 506-520.
802 Wackrow, R. and Chandler, J., 2008 A convergent image configuration for DEM extraction
803 that minimises the systematic effects caused by an inaccurate lens model. The
804 Photogrammetric Record, 23121, 6-18.
805 Wilcock, P., 1996. Estimating local bed shear stress from velocity observations. Water
806 Resour. Res. 3211, 3361 - 3366.
807 Zhang, W., and Montgomery, D. R., 1994. Digital Elevation Model Grid Size, Landscape
808 Representation, and Hydrologic Simulations. Water Resour. Res., 304, 1019-1028.
809 Zhang, Z., 2000. A Flexible New Technique for Camera Calibration. IEEE Trans. Pattern
810 Anal. Mach. Intell., 2211, 1330-1334.
811
812
813